Mississippi State University
Scholars Junction

Theses and Dissertations | Theses and Dissertations

8-7-2020

Advanced in-situ layer-wise quality control for laser-based additive manufacturing using image sequence analysis

Mehrnaz Noroozi Esfahani

Follow this and additional works at: https://scholarsjunction.msstate.edu/td

Recommended Citation
Noroozi Esfahani, Mehrnaz, "Advanced in-situ layer-wise quality control for laser-based additive manufacturing using image sequence analysis" (2020). *Theses and Dissertations*. 402.
https://scholarsjunction.msstate.edu/td/402

This Graduate Thesis - Open Access is brought to you for free and open access by the Theses and Dissertations at Scholars Junction. It has been accepted for inclusion in Theses and Dissertations by an authorized administrator of Scholars Junction. For more information, please contact scholcomm@msstate.libanswers.com.

www.manaraa.com

Advanced in-situ layer-wise quality control for laser-based additive manufacturing using image sequence analysis

By

Mehrnaz Noroozi Esfahani

Approved by:

Wenmeng (Meg) Tian (Major Professor)
Nazanin Morshedlou
Junfeng Ma
Linkan Bian (Graduate Coordinator)
Jason M. Keith (Dean, Bagley College of Engineering)

A Thesis
Submitted to the Faculty of
Mississippi State University
in Partial Fulfillment of the Requirements
for the Degree of Master of Science
in Industrial Engineering
in the Department of Industrial and Systems Engineering

Mississippi State, Mississippi

August 2020

www.manaraa.com

Copyright by

Mehrnaz Noroozi Esfahani

2020

www.manaraa.com

Name: Mehrnaz Noroozi Esfahani

Date of Degree: August 7, 2020

Institution: Mississippi State University

Major Field: Industrial Engineering

Major Professor: Wenmeng (Meg) Tian

Title of Study: Advanced in-situ layer-wise quality control for laser-based additive manufacturing using image sequence analysis

Pages in Study 29

Candidate for Degree of Master of Science

Quality assurance has been one of the major challenges in laser-based additive manufacturing (AM) processes. This study proposes a novel process modeling methodology for layer-wise in-situ quality monitoring based on image series analysis. An image-based autoregressive (AR) model has been proposed based on the image registration function between consecutively observed thermal images. Image registration is used to extract melt pool location and orientation change between consecutive images, which contains sensing stability information. Subsequently, a Gaussian process model is used to characterize the spatial correlation within the error matrix. Finally, the extracted features from the aforementioned processes are jointly used for layer-wise quality monitoring. A case study of a thin wall fabrication by a Directed Laser Deposition (DLD) process is used to demonstrate the effectiveness of the proposed methodology.

www.manaraa.com

DEDICATION

"We cannot all succeed when half of us are held back."

Malala Yousafzai

I dedicate my thesis work to my family. A special feeling of gratitude to my loving parents and my sister who have supported me throughout the process.

www.manaraa.com

ACKNOWLEDGEMENTS

Research was sponsored by the Army Research Laboratory and was accomplished under Cooperative Agreement Number W911NF-15-2-0025. The views and conclusions contained in this document is those of the authors and should not be interpreted as representing the official policies, either expressed or implied, of the Army Research Laboratory or the U.S. Government. The U.S. Government is authorized to reproduce and distribute reprints for Government purposes notwithstanding any copyright notation herein. Also, I would like to thank Dr. Wenmeng Tian, the chair of my Ph.D. Committee, whose guidance and Help lead my master's program.

www.manaraa.com

TABLE OF CONTENTS

www.manaraa.com

LIST OF TABLES

www.manaraa.com

LIST OF FIGURES

www.manaraa.com

CHAPTER I

INTRODUCTION

Additive Manufacturing (AM) processes add material in layer-by-layer fashion to achieve the final geometry, which enables new design options that cannot be obtained through conventional manufacturing technologies [1]. Nevertheless, quality issues of AM parts are major barriers preventing wider industrial adoption of AM. Due to the existence of defects such as porosity and cracking, the mechanical properties of additively manufactured parts can hardly satisfy the strict requirements of industrial application. AM processes are governed by the process-structure-property (PSP) relationship. Once the PSP relationship is established, the build structure and properties can be predicted. Direct Laser Deposition (DLD), is one of Laser Based Additive Manufacturing methods that melts the powder or wire as row material by irradiation of a laser beam. The melt-pool (or molten pool) is created when metal powder/wire delivered to a mobile substrate is simultaneously exposed to a relatively high-powered laser. As illustrated in Figure 1.1 a focused laser beam irradiated laser using turning mirrors in one direction with a single powder-spray nozzle or multiple nozzles. The thermal energy produced by laser melts the material (powder or wire) injected on the substrate. That creates the molten metal on top of a heat affected zone (HAZ) [2], [3]. However, wire-fed DLD is sometimes regarded as a more efficient way since Powder preform is injected through nozzle that can cause an agglomerate of remained powder. However, wire-fed DLD is sometimes regarded as a more efficient way since powder preform is injected through nozzle that can cause an agglomerate of remained powder [4].

www.manaraa.com

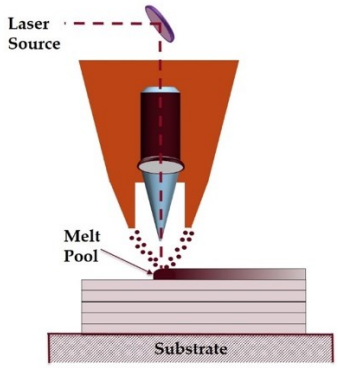

Figure 1.1 Direct laser deposition schema

The challenges confronting layer-based process anomaly detection are two-fold: 1) there is a huge amount of uncertainty in the relationship between the compositional and process parameters in the basic thermo-mechanical process of metal printing; 2) the advanced sensing technologies provide high volume of noisy thermal history data that represent complex spatio-temporal relationship. To model correlation between thermal history and microstructure properties, finite element methods (FEMs) have been widely used. The thermal behavior and temperature distribution and their effects on the stress, formation, and hardness of parts along with phase transformation during the AM process have been thoroughly studied in the literature [2,3]. However, there are some challenges in the FEM based approaches that hinder their application in online prediction [4]: 1) high computational cost required, making it extremely time consuming to implement in real time; 2) their high dependency on part geometry which makes it almost impossible to generalize between different designs; and 3) the deterministic nature of FEM related approaches, making it difficult to incorporate all sources of process uncertainty in the modeling for anomaly detection.

www.manaraa.com

The advancement in sensing technologies has enabled real-time monitoring of thermal history for anomaly detection via infrared thermography, generating thermal imaging data streams with extremely large volume and complex structure. Although existing data-driven methods consider robust statistical methods to identify anomalies from thermal image [5-6], local features for prediction purposes are used in most of the existing work and, consequently, they cannot be directly utilized to distinguish the profile of an entire deposited layer. This being the case, layer-wise process signature has received the attention of the AM community. Liu et al. [7] has modeled layer-wise spatial porosity evolution based on X-ray computed tomography (XCT), which is an expensive and time-consuming process. Furthermore, optical imaging systems have been used in laser powder bed fusion systems for layer-wise monitoring [8]. Moreover, layer-wise anomaly detection based on thermal history has also been proposed which incorporates a tensor-based dimension reduction and a convex-hull based variability characterization approach [9].

The melt pool images are regarded as a most informative process signature for build structure prediction. Figure 1.2 shows a schematic plot of a Direct Laser Deposition Process (DLD) fabrication process monitored by a coaxial pyrometer. It is observed that whenever there is a shift occurring in the process, a significant change can be observed in the series of melt pool images captured in fabricating that shifted layer. Therefore, we propose to formulate the layer-wise thermal history as an image-based time series for layer-wise anomaly detection in the in-situ DLD process monitoring.

In this study, a novel data-driven methodology is proposed to extract layer-wise process signatures from real-time thermal history for direct laser deposition (DLD) processes. AM process knowledge is leveraged to develop the novel approach. Therefore, the major assumption of the proposed methodology is that a stable thermal history leads to homogenous microstructure and

www.manaraa.com

thus porosity-free deposited layers. As illustrated in Figure 1.2, when there is a layer height anomaly occurring in the process, the observed melt pool in the thermal image will shift in both shape and location. Based on this observation, process features can be proposed to quantify the change in the thermal image series obtained from fabricating one layer. Therefore, process features can be extracted from two sources in the thermal image series, 1) image registration information; and 2) first order difference of the registered thermal images. Subsequently, the extracted features are used for anomaly detection for each deposited layer in the DLD process.

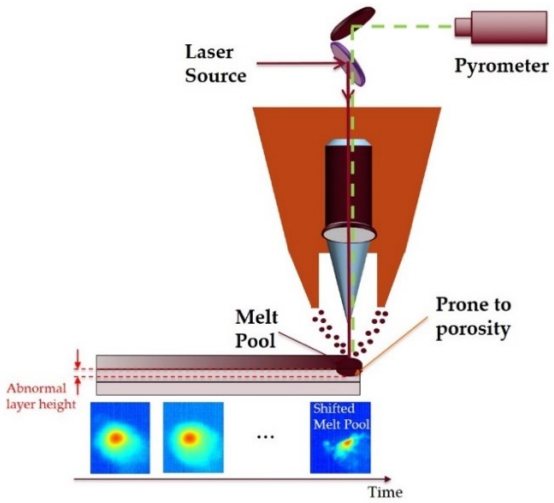

Figure 1.2 DLD process monitored by a co-axial pyrometer

The rest of the study is structured as follows. chapter 2 provides a detailed literature review on the existing porosity detection techniques, following that the efforts on characterization of melt pool are briefly discussed. In chapter 3 the proposed framework for layer-wise process feature extraction and anomaly detection, while chapter 4 presents a case study of fabricating a thin wall

www.manaraa.com

using a DLD process to validate the proposed methodology. Finally, chapter 5 summarizes the conclusion and potential future research directions.

www.manaraa.com

CHAPTER II

LITERATURE REVIEW

In this chapter, the state-of-the-art research on porosity detection and characterization for laser-based additive manufacturing is categorized into four groups, with each summarized in one subsection as follows.

2.1 Post-manufacturing porosity detection and characterization

Several studies focus on post-manufacturing inspection. Computed Topography (CT) and Magnetic Resonance Imaging (MRI) are used to detect the internal defects in the product as well as the measurement of shifts from designed model [5]. Du Plessis et al, investigated the measurement of minimum detectable pore size regarding CT adjustment, which reveals the advantages of additive manufacturing over casting [6]. Porosity characterization in casting process has been discussed by Wilczek, in which they analyzed non-destructive tests including ultrasonic, radiographic, eddy current and pulsed infrared thermography for performance comparison [7].

Due to the widespread use of additive manufacturing, there has been an increasing demand for the efficient methods to control the quality of products, Bernier et al. used X-ray tomography combined with 3D image analysis and they evaluated the effect of the parameters of X-ray tomography on image quality. The study also validated XCT for the porosity detection challenge in additive manufacturing powder feedstock [8].

Moreover, Chen et al. created a comprehensive comparison between three types of spherical Ti-6Al-4V powders in terms of microstructure, porosity, argon gas content and pore

www.manaraa.com

spatial structure. They demonstrated that Synchrotron X-ray CT is a more beneficial tool to characterize pore morphology due to the high-resolution of this technology. Also, the analyzing of three-dimensional reconstructed images shows that any increase in the pore population, size and porosity within powders leads to moderately increase in particle size[9].

Many efforts have been done to improve the quality through collecting valuable data, therefore different methods have been used to obtain the data including porosity. Cnudde et al. compared 3 techniques of porosity data collection including water intrusion porosimetry, micro-CT and water absorption under vacuum, besides, advantages and disadvantages of these 3 techniques were discussed [10]. In other works, it has been concluded that depending on pore size and pore structure, mercury intrusion porosimetry results can be more or less illustrative [11].

When it comes to process optimization and quality control for AM production, post-manufacturing quality control approaches are usually very expensive, and sometimes even destructive. Furthermore, it is worth noting that the post-manufacturing approaches, sometimes also called offline approaches, can be adopted only after the product is fabricated. Therefore, those techniques cannot facilitate in-situ decision making and process adjustment during the AM process to improve part quality [12].

2.2 Melt-pool thermodynamics, monitoring and modeling

Due to the widespread use of laser welding process, Mazumder et al. (1996) collected modelling studies on laser heat treatment including Directed Energy Deposition processes. The study shows the remarkable effect of heat transfer and fluid flow in the weld pool on the characteristics of the weld seam produced by the laser welding in DED process including microstructure, distortion, residual stress, etc. [13].

www.manaraa.com

A multivariate model is stablished by Wang et al., which emphasizes the impact of material transfer rate parameters for directed energy deposition. The steady-state melt-pool geometry and temperature are also predicted using the model [14].

Letenneur et al. studied the laser powder bed fusion (LPBF) process and stablished a density prediction algorithm. Certain range of values are considered for manufacturing parameters including laser power, scanning speed, hatching space, and layer thickness. Densities of fabricated parts has been calculated as response value and the melt pool dimensions are measured using a simplified melt pool model. and the gathered data were analyzed to predict the density of printed parts [15].

Heat transfer and residual stress evolution in the direct metal laser sintering process are assessed by Zhao et al. regarding the temperature-based features of TiAl6V4. Also, a 2-D model and a 3-D model are developed to analyze the single- layer laser sintering and multi-layer effects consequently. melt pool size, temperature history, and change of the residual stresses of a single layer and among the multiple layers of the effects of the change of the local base temperature and laser power etc. The study shows the changes in melt pool size, temperature history and residual stress of each layer individually [16].

For processing of laser powder bed fusion, an integrated physics-based and statistical modeling approach is developed by Criales et al. to predict temperature field and melt-pool geometry. Temperature fields during the scan and hatch directions have been simulated using 2-D finite element simulations which helps to characterize the melt-pool changes [17].

Konrad Bartkowiak, and Mikhail Vasiley have studied the feasibility of applying real time monitoring spectroscopy for different solid state and CW laser systems. Using online digital imaging the spectra emission lines are recorded which explains the changes in melt pool

www.manaraa.com

composition during DLD process. The image processing delivers remarkable information including size and shape changes of the plasma plume and melt pool during laser irradiation on metal powder [18].

The importance of recoil pressure and Marangoni convection in shaping the melt pool flow in studied by Khairallah et al. Also, the laser bed-fusion process is analyzed to find how the denudation, spattering, and pore defects appear in the surface of fabricated part. They finally concluded that in order to reduce porosity, deep and narrow depressions should be prevented, laser intensity should decrease when the direction changes along a scan track [19].

Thermomechanical simulations are widely used to study the behavior of melt-pools during solid freeform fabrication (SFF) processes. Process maps are sort of quasi-non-dimensional plots which are developed by Thermal simulations in order to quantifies the effects of changes on melt pool length over the full range of relevant process variables [20]. Vasinonta et al utilized Process maps to reduce the residual stress by adjusting a set values for production parameters including wall height, laser power, deposition speed, and part preheating. The recommended strategy at this study for obtaining an optimal melt pool size is to uniformly preheat the part to reduces the stress, also, applying slight reductions in laser power or increases in laser velocity [20]. Moreover, Gockel et al. utilized using finite element analysis to investigate a solidification microstructure process map. At this study a proportional size scaling between beta grain widths and melt pool widths has been recognized and finally it is indicated that controlling the melt pool dimension control enables to control solidification microstructure [21].

Geometrical accuracy is one of functional features that helps to characterize the thermal behavior of molten pool in order to distinguish between healthy and non-healthy melt-pools. Hu and Kovacevic investigate a three-dimensional finite element model using ANSYS to study the

www.manaraa.com

thermal behavior of the molten pool for building a single bead stainless steel wall while the laser power is controlled to keep the width of the molten pool constant [22].

2.3 Melt-pool characterization and monitoring based on in-situ measurements

There are two types of measurements that can be used for anomaly detection in laser based additive manufacturing systems, optical imaging sensors and thermal imaging sensors. Helaric et al. recommends camera-based feedback for on-line control of the laser metal wire deposition, however, with certain caution due to measurement disturbances. The melt pool width is obtained using an optic camera [23]. Hu and Kovacevic developed a close-loop control system based on infrared image sensing to characterize the molten pool in Laser Based Additive Manufacturing process. The system is consisting of a high frame rate camera located above the laser head that captures gray images [24].

Thermal imaging has been used as an efficient tool for anomalies detection both in online monitoring and for part inspection. The porosity inside the part can be detected through image processing which helps to control the final quality. Khanzadeh et al. developed a method to characterize the melt pool by processing thermal images. The images of ill-structured melt pools have been fed to the supervised learning method to predict the porosity in single track thin walls fabricated by direct laser deposition [25]. For the same purpose, Seifi et al. analyzes thermal images provide by a co-axial pyrometer camera. In order to label the data, the melt pools locations have been matched with corresponding XCT scanning images which detects the porosity inside the part [26].

It is worth noting that most of the existing studies focus on post-manufacturing porosity prediction that is less effective comparing with online monitoring in terms of process cost. Furthermore, in situ monitoring can help to uncover the causes of defects while post-

www.manaraa.com

manufacturing is destructive. Khanzadeh et al. proposed a method to model the non-healthy melt pool by quantifying and characterizing the temperature distribution of the top surface of the melt pool. The model is capable of detecting process anomalies in the noisy melt pool signals during the manufacturing process [27].

2.4 Video analysis for additive manufacturing monitoring

The widespread use of machine vision systems in additive manufacturing technologies could lead to the demand for image-based statistical process monitoring methods. Moreover, large amounts of data generated in new formats (i.e., video images) captured at high speed needs could be analyzed via big data methods in order to detect and predict the defect during production.

Colosimo and Grasso proposed a novel approach based on spatially weighted PCA (Principal Component Analysis) characterizing the spatiotemporal features of the process represented in the monitored video image data. Also, the k-means clustering-based is applied to develop an alarm rule which is capable of automatic defect detection [28]. Yan et al. suggested a decomposition-based approach with the aim of real time monitoring and anomaly detection. Therefore, Video-imaging data are processed to extract features through spatio-temporal variability in order to decompose the original data into random natural events, sparse spatially clustered and temporally consistent anomalous events, and random noise [29].

However, those methods are mostly pure data-driven methods which do not take into account the AM process knowledge in the analysis.

www.manaraa.com

CHAPTER III

METHODOLOGY AND MODELING

3.1 Data description and challenges

Thermal history indicates the thermal response during AM fabrication as a function of time, which is represented by an image series (video) captured by a pyrometer camera during the build. In the thermal images, a region of superheated molten metal is defined as the melt pool [3]. As a key signature of the fabrication process, the melt pool initiates the solidification process in AM and thus is informative to predict part porosity information. Each melt pool image contains location-based temperatures, and each layer can be considered as a series of images. Most of the currently available approaches use individual melt pool image for anomaly detection at the specific location where the melt pool is observed during the fabrication. However, plenty of spatio-temporal correlation information presents in the image series which can be used for anomaly detection and quality prediction. The monitoring of layer-wise thermal history is challenging due to 1) complex spatio-temporal correlation, 2) high dimensionality of thermal images, 3) discrete data sampling, and 4) unreliable and missing data.

3.2 Thermal image series analysis

In this subsection, the proposed framework for modeling the thermal image series collected from fabricating one layer is briefly described. A thermal image time series collected from fabricating one layer can be modeled as an image-based autoregressive model,

www.manaraa.com

$$X_{t+1} = f_{t+1}(X_t, \mathbf{\Omega}_t) + \varepsilon_{t+1} \tag{3.1}$$

where X_t denotes the thermal image with a dimension of $I \times J$ collected at time stamp t ($t = 1,2, \dots, T_l - 1$) in which T_l denotes the number of images collected when fabricating the l-th layer. It is worth noting that T_l is possible to vary for different layers; f_{t+1} is an image registration function between X_t and X_{t+1} in one layer characterized by a 3×3 transformation matrix $\mathbf{\Omega}_t$. ε_{t+1} denotes an error matrix (with a dimension of $I \times J$) representing the piece of information that cannot be explained by the registration operation. A Gaussian process model is used here to characterize the error term ε_{t+1}, and the detailed information is included in subsection 1.3.4. Figure 3.1 shows the consecutive melt pool images as an image series, and briefly illustrates the proposed formulation in Equation (3.1).

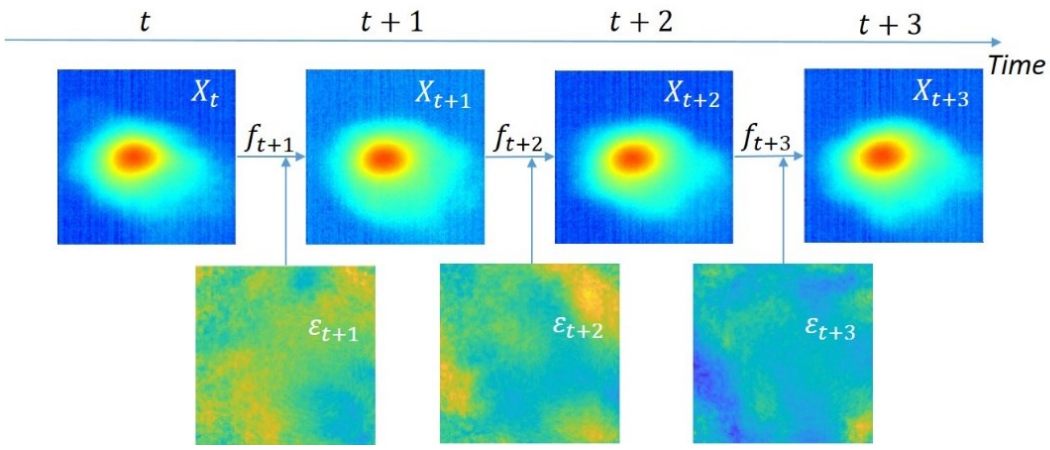

Figure 3.1 Layer-wise thermal image series formulation

www.manaraa.com

3.3 Image registration

Image registration is a widely used image processing technique that reveals some hidden relationship between the input and the reference images in applications such as health care industry [30], computer vision for target localization, automatic quality control, motion tracking, and cartography for map updating. A registration function is usually in the form of a coordinate transformation matrix.

In this study, image registration is used to project X_t to X_{t+1} $(t = 1,2, \dots, T_l - 1)$ for the best alignment, and each registration function f_t can involve operations including translation and rotation. More specifically, translation describes the shift magnitude in a 2D coordinate system between X_t and X_{t+1}; rotation describes the orientation difference between X_t and X_{t+1}. The image registration algorithm is performed in an iterative procedure to optimize a pre-defined similarity metric (such as mean square error). The image operations iteratively modify X_t to best match X_{t+1} for a smaller mean squared error. The result of the image registration procedure is specified as a 3×3 transformation matrix $\mathbf{\Omega}_t$ as follows,

$$\mathbf{\Omega}_t = \begin{bmatrix} a & b & 0 \\ c & d & 0 \\ t_x & t_y & 1 \end{bmatrix} \tag{3.2}$$

where a, b, c, and d jointly specify the rotation operations, and t_x and t_y denote the number of pixels to shift the image in the horizontal and vertical direction, respectively. More specifically, two possible special cases of $\mathbf{\Omega}_t$ are discussed as follows.

Case 1: When $b = c = 0, and\ a = d = 1$, $\mathbf{\Omega}_t$ specifies a registration function with a translation operation only;

www.manaraa.com

Case 2: When a, b, c, and d satisfy $a = d = \cos q \ and \ b = -c = \sin q$ where q represents the angle of rotation about the origin of the image, $\boldsymbol{\Omega}_t$ specifies a registration function with both rotation and translation operations;

3.4 Gaussian process model

Gaussian Process (GP) modeling technique has an advantage to develop the model with the help of identifying the structure of the covariance matrix of the explanatory variables. This feature makes the GP model more flexible than traditional approaches, which consider only the algebraic structure of the input–output relationship. Therefore, the GP model is able to capture strong nonlinearities and multivariate interactions in a systematic way. Derived from a Bayesian setting, the GP enables to combine and quantify separate sources of uncertainty in a natural way [31].

The error term ε_t in Equation (3.1) is modeled as follows,

$$\varepsilon_t \sim GP\left(\beta_t, K\left((i,j),(i',j')\right) + \sigma_t^2 I\right) \tag{3.3}$$

where i and j denote the row and column indices of the pixel in the error term matrix ε_t $i = 1,2,3,\dots,I, and \ j = 1,2,3,\dots,J$. β_t represents the mean of the Gaussian process ε_t, whereas σ_t^2 shows the white noise variation of pixels. $K(\cdot,\cdot)$ represents the kernel function used to characterize the covariance between the two different locations, i.e. (i,j) and (i',j'). In Gaussian processes, the covariance function characterizes the correlation (similarity) between neighboring pixels within the ε_t matrix, which obviously have similar response values. In other words, it determines how the response at each pixel is affected by responses at other pixels. The covariance

www.manaraa.com

function $K(\cdot,\cdot)$ can be defined by various kernel functions, which can be parameterized in terms of different kernel parameters.

In this study, Matern 3/2 covariance kernel function is used to characterize the spatial correlation in ε_t's as follows,

$$K\left((i,j),(i',j')|\sigma_l,\sigma_f\right) = \sigma_f^2(1+\frac{\sqrt{3}r}{\sigma_l})\exp\,(-\frac{\sqrt{3}r}{\sigma_l}) \tag{3.4}$$

where r is the Euclidean distance between the two pixels (i,j) and (i',j'), i.e., $r = \sqrt{(i-i')^2+(j-j')^2}$, as illustrated in Figure3.2; σ_l is the characteristic length scale, and σ_f is the signal standard deviation [32]. It is worth noting that Quasi-Newton optimizer is used for parameter estimation in the GP.

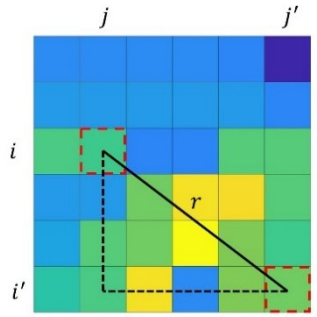

Figure 3.2 Distance between pixels in a thermal image

www.manaraa.com

3.5 Layer-wise feature extraction

There are two groups of features extracted to characterize the thermal image series: one is extracted from the transformation matrix obtained from the registration function, and the other is extracted from the estimated parameters from the GP models to characterize the error matrix.

Image registration related features are extracted from the transformation matrix $\mathbf{\Omega}_t$. Without losing generality, it is assumed that the transformation can be achieved by a sequence of image operations as rotation and translation, i.e.,

$$\mathbf{\Omega}_t = \begin{bmatrix} a & b & 0 \\ c & d & 0 \\ t_x & t_y & 1 \end{bmatrix} = \mathbf{\Omega}_t^{\mathrm{R}} \times \mathbf{\Omega}_t^{\mathrm{T}} \tag{3.5}$$

where the rotation and translation parameters can be identified: 1) the rotation angle $q = \tan^{-1}\left(\frac{b}{a}\right)$; 2) the translation in horizontal and vertical directions are t_x and t_y, respectively.

Two features can be extracted from parameter q, t_x and t_y. In order to extract a feature from translation, t_x and t_y are used to calculate the Euclidian distance shifted from the original image and registered image as follows,

$$ED_{l,t} = \sqrt{t_x^2 + t_y^2} \tag{3.6}$$

In order to modify this variable for layer-wise prediction, the maximum of $ED_{l,t}$'s over the consecutive image pairs of a layer is considered, Therefore, the feature extracted from image registration translation will be presented as

www.manaraa.com

$$F_l^1 = \max_{1 \le t \le T_l - 1} \{ED_{l,t}\} \tag{3.7}$$

Similarly, the feature to characterize the rotation operation can be calculated as

$$F_l^2 = \max_{1 \le t \le T_l - 1} \{|q_{l,t}|\} \tag{3.8}$$

The next category of features is extracted by parameters of GP model which are defined as $F_{l,t}^3 = \beta_t$ which is the maximum of β over images of a layer, $F_{l,t}^4 = \sigma_t$ and $F_{l,t}^5 = \sigma_{t,L}$; $F_{l,t}^6 = \sigma_{t,f}$ which are based on variation of pixels, characteristic length scale and the signal standard deviation, respectively. Again the maximum of each feature for a single layer is calculated to obtain the layer-wise features as $F_l^i = \max_{1 \le t \le T_l - 1} \{F_{l,t}^i\}$, where $i = 3, 4, 5, 6$.

It is worth noting that when coaxial thermal monitoring systems are used, the location of the melt pools does not change over time under the normal processing condition. Therefore, Eq. (5) works for all different printing paths. However, Eq. (6) works only when the printing path is unidirectional, where the theoretical rotation angle equals to 0. However, for complicated scanning path, the calculated rotation parameter needs to be compared with the theoretical rotation based on the designed scanning path. As illustrated in Figure3.3, the moving direction of laser is changing over the time. In that case, F_l^2 feature is calculated as follows,

$$F_l^2 = \max_{1 \le t \le T_l - 1} \{|q_{l,t} - \Delta\theta_{t,t+1}|\} \tag{3.9}$$

www.manaraa.com

where $\Delta\theta_{t,t+1}$ represents the theoretical rotation angle between the two consecutive melt pools. An example is shown in Figure3.3 in which two melt pools observed in a same layer have different moving directions, where $\Delta\theta_{t,t+1} = \theta_{t+1} - \theta_t$. In other words, Eq. (7) is the general form of Eq. (6). The features from the error term apply to all different scanning paths as all the assignable changes should be incorporated in the registration operation.

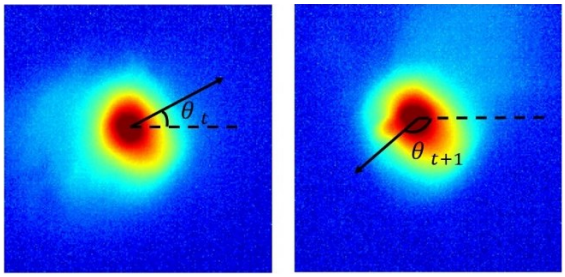

Figure 3.3 Consecutive thermal images with different moving direction

3.6 Classification: Correlating layer signatures to structural quality

When structural quality information, such as X-ray CT scanned results, is available. Supervised learning methods can be used to train a classification model. Support Vector Machine (SVM) is considered as a powerful classification technique with a diversity of kernel functions. By finding the best hyperplane that separates all data points of different classes, an SVM classifier can be trained using data labeled with X-ray CT evaluations. More specifically, a layer that contains at least one porosity is labeled as unhealthy, and a porosity-free layer is labeled as healthy. Among SVM classifiers, linear SVM is applied in this paper for simplicity and better interpretability. To achieve more flexibility, more sophisticated kernels such as Gaussian kernel or polynomial kernel can be used [33]. It is worth noting that various other machine learning

www.manaraa.com

algorithms can also be applied to this problem. Comparing classification performance of different machine learning schemes is out of the scope of this study.

www.manaraa.com

CHAPTER IV

CASE STUDY

The performance of the proposed methodology is validated using a direct laser deposition process. A thin wall of 60 layers in total was fabricated using Ti-6AL-4V. During the fabrication, the thermal images of the melt pools related to different locations on the thin wall are captured by a pyrometer camera. The number of thermal images captured using co-axial pyrometer camera is 1564 with each represented by a 480 $\times$ 752 matrix of pixels. The process setup parameters are summarized in Table 4.1 [34]. After the build was completed, the porosity structure inside the build was identified using an X-ray CT scan (Skyscan 1172). The X-ray examination indicated that 26 layers out of 60 layers of the thin wall include at least one porosity. Figure 4.1 illustrates a melt pool image series within a layer containing a porosity related to an unhealthy melt pool at t+17. It is worth noting that minimum size for a pore is 0.05μm.

Table 4.1 LENS process design parameters for the thin wall.

Scan speed	12.70 mm/s	Starting offset from substrate	130.391mm
Powder feed rate	0.060 g/s	Determination of layer thickness	0.508 mm
Determination of hatch spacing	0.508 mm	Nozzle diameter	0.889 mm
Power	300 W	Substrate (stainless steel)	3.175 mm

www.manaraa.com

For image registration, due to the printing path design was unidirectional, the orientation of the melt pool image should not change over time. Therefore, only translation operation is estimated in the transformation matrix $\mathbf{\Omega}_t$. Fabricating a thin wall, the melt pool only shifts from image to image and the melt pool is not subjected to rotation. Regarding that the only transformation that can be applicable is translation, the feature extracted from translation are the only feature extracted from the image registration process. The error term ε_t's was modeled using Gaussian process models, and the layer-wise features were obtained by calculating the maximum values for each feature.

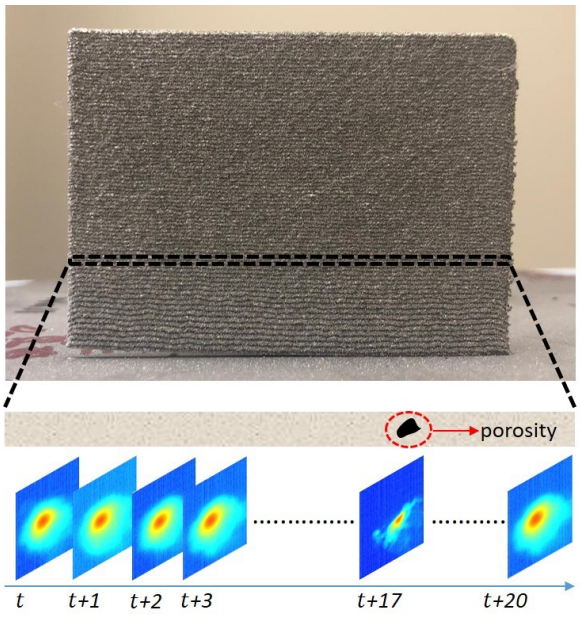

Figure 4.1 The image of a thin wall containing one pore in an unhealthy layer

Leave-one-out validation was used to test the effectiveness of the proposed method. Table 4.2 illustrates the confusion matrix after implementing the aforementioned model. Four layers out of 60 layers (6.67% of the total layers) are misclassified, in which two misclassifications for

www.manaraa.com

healthy and two for unhealthy. The recall, precision, and *F*-score were considered as three measures to define the accuracy of the model and calculated as follows:

$$Recall = \frac{TP}{TP + FN} \tag{4.2}$$

$$Precision = \frac{TP}{TP + FP} \tag{4.2}$$

$$F - score = 2 \times \frac{Precision \times Recall}{Precision + Recall} \tag{4.3}$$

where F-score is the harmonic mean of precision and recall. TP shows true positive layers which are unhealthy and predicted accurately as unhealthy. TN stands for true negative that illustrated the items that are accurately predicted as healthy. On the other hand, FN defines inaccurate prediction that are actually unhealthy, while FP shows inaccurate prediction that are actually healthy.

Table 4.2 Confusion matrix for leave-one-out cross validation

		Predicted	
		Healthy	Unhealthy
Actual	Healthy	32	2
	Unhealthy	2	24

www.manaraa.com

The results indicate that the recall and precision of leave-one-out cross validation are 0.9231 and 0.9231, respectively, and consequently, the *F*-score is also 0.9231. This indicates that the classification model accuracy is reasonably high and can be used for layer-wise anomaly detection. One of the possible reasons for misclassification is the discrete data sampling for thermal history fails to capture the thermal image when the anomaly occurs. Consequently, some information will be missed. In addition, the X-ray CT scans may be subject to noise and error as well. Moreover, the proposed anomaly detection method does not consider effects of re-melting, which can potentially correct some of the porosities generated in the previous layer.

www.manaraa.com

CHAPTER V

CONCLUSION AND FUTURE WORK

Lack of repeatability in the additively fabricated parts is one of the major challenges that hinders broader industrial applications of additive manufacturing processes. Possible build quality issues, such as internal porosity, deformation, and cracking, can lead to significantly compromised mechanical properties. Comprehensive studies including data-driven methods have been focused on local characterization for anomaly detection based on single thermal images. A layer-wise thermal image modeling framework can take into account the complex spatio-temporal relationship within the image series, which can potential achieve improved anomaly detection results. In this paper, the layer-wise thermal images are formulated as an image series, and an image-based autoregressive (AR) model has been proposed based on the registration function between consecutively observed thermal images. Multiple features are extracted from the AR model for each consecutive pair of images, and layer-wise features are extracted subsequently. Support Vector Machine method is used for anomaly detection based on the extracted layer-wise features. A case study based on a thin wall fabrication using a DLD process is used to validate the proposed methodology. The classification accuracy of the proposed method is reasonably high which makes the model capable of predicting defects. For future works, the represented model can be applied to the thermal image analysis of AM parts with more complicated geometry to evaluate the performance of the proposed method. Also, the tensor-based calculations can be used to take the advantage of matrix-based structure of data.

www.manaraa.com

REFERENCES

[1] M. Grasso and B. M. Colosimo, "Process defects and in situ monitoring methods in metal powder bed fusion: a review," *Measurement Science and Technology*, vol. 28, no. 4, p. 044005, Feb. 2017, doi: 10.1088/1361-6501/AA5C4F.

[2] N. Shamsaei, A. Yadollahi, L. Bian, and S. M. Thompson, "An overview of Direct Laser Deposition for additive manufacturing; Part II: Mechanical behavior, process parameter optimization and control," *Additive Manufacturing*, vol. 8. Elsevier B.V., pp. 12–35, Oct. 01, 2015, doi: 10.1016/j.addma.2015.07.002.

[3] S. M. Thompson, L. Bian, N. Shamsaei, and A. Yadollahi, "An overview of Direct Laser Deposition for additive manufacturing; Part I: Transport phenomena, modeling and diagnostics," *Additive Manufacturing*, vol. 8. Elsevier B.V., pp. 36–62, Oct. 01, 2015, doi: 10.1016/j.addma.2015.07.001.

[4] M. L. Griffith *et al.*, "Understanding thermal behavior in the LENS process," *Materials and Design*, vol. 20, no. 2–3, pp. 107–113, Jun. 1999, doi: 10.1016/s0261-3069(99)00016-3.

[5] H. Kim, Y. Lin, and T. L. B. Tseng, "A review on quality control in additive manufacturing," *Rapid Prototyping Journal*, vol. 24, no. 3, pp. 645–669, 2018, doi: 10.1108/RPJ-03-2017-0048.

[6] A. du Plessis, S. G. le Roux, G. Booysen, and J. Els, "Quality Control of a Laser Additive Manufactured Medical Implant by X-Ray Tomography," *3D Printing and Additive Manufacturing*, vol. 3, no. 3, pp. 175–182, 2016, doi: 10.1089/3dp.2016.0012.

[7] A. Wilczek, P. Długosz, and M. Hebda, "Porosity Characterization of Aluminium Castings by Using Particular Non-destructive Techniques," *Journal of Nondestructive Evaluation*, vol. 34, no. 3, pp. 1–7, 2015, doi: 10.1007/s10921-015-0302-z.

[8] F. Bernier, R. Tahara, and M. Gendron, "Additive manufacturing powder feedstock characterization using X-ray tomography," *Metal Powder Report*, vol. 73, no. 3, pp. 158–162, 2018, doi: 10.1016/j.mprp.2018.01.002.

[9] G. Chen *et al.*, "A pore morphological study of gas-atomized Ti-6Al-4V powders by scanning electron microscopy and synchrotron X-ray computed tomography," *Powder Technology*, vol. 330, pp. 425–430, 2018, doi: 10.1016/j.powtec.2018.02.053.

www.manaraa.com

[10] V. Cnudde, A. Cwirzen, B. Masschaele, and P. J. S. Jacobs, “Porosity and microstructure characterization of building stones and concretes,” *Engineering Geology*, vol. 103, no. 3–4, pp. 76–83, 2009, doi: 10.1016/j.enggeo.2008.06.014.

[11] G. F. Andriani and N. Walsh, “Fabric, porosity and water permeability of calcarenites from Apulia (SE Italy) used as building and ornamental stone,” *Bulletin of Engineering Geology and the Environment*, vol. 62, no. 1, pp. 77–84, 2003, doi: 10.1007/s10064-002-0174-1.

[12] M. Khanzadeh, W. Tian, A. Yadollahi, H. R. Doude, M. A. Tschopp, and L. Bian, “Dual process monitoring of metal-based additive manufacturing using tensor decomposition of thermal image streams,” *Additive Manufacturing*, vol. 23, no. August, pp. 443–456, 2018, doi: 10.1016/j.addma.2018.08.014.

[13] J. Mazumder, “Advanced laser processing of metals,” in *LEOS Summer Topical Meeting*, 1996, doi: 10.1109/leosst.1996.540662.

[14] Q. Wang, J. Li, M. Gouge, A. R. Nassar, P. Michaleris, and E. W. Reutzel, “Physics-Based Multivariable Modeling and Feedback Linearization Control of Melt-Pool Geometry and Temperature in Directed Energy Deposition,” *Journal of Manufacturing Science and Engineering, Transactions of the ASME*, vol. 139, no. 2, pp. 1–12, 2017, doi: 10.1115/1.4034304.

[15] M. Letenneur, A. Kreitcberg, and V. Brailovski, “Optimization of Laser Powder Bed Fusion Processing Using a Combination of Melt Pool Modeling and Design of Experiment Approaches: Density Control,” *Journal of Manufacturing and Materials Processing*, vol. 3, no. 1, p. 21, 2019, doi: 10.3390/jmmp3010021.

[16] X. Zhao, A. Iyer, P. Promoppatum, and S. C. Yao, “Numerical modeling of the thermal behavior and residual stress in the direct metal laser sintering process of titanium alloy products,” *Additive Manufacturing*, vol. 14, pp. 126–136, 2017, doi: 10.1016/j.addma.2016.10.005.

[17] L. E. Criales, Y. M. Arısoy, B. Lane, S. Moylan, A. Donmez, and T. Özel, “Predictive modeling and optimization of multi-track processing for laser powder bed fusion of nickel alloy 625,” *Additive Manufacturing*, vol. 13, pp. 14–36, 2017, doi: 10.1016/j.addma.2016.11.004.

[18] K. Bartkowiak and M. Vasiley, “Direct laser deposition - A comparative study using different CW YAG lasers and with in situ real-time spectroscopy and imaging,” *26th International Congress on Applications of Lasers and Electro-Optics, ICALEO 2007 - Congress Proceedings*, vol. 403, 2007, doi: 10.2351/1.5061068.

[19] S. A. Khairallah, A. T. Anderson, A. Rubenchik, and W. E. King, “Laser powder-bed fusion additive manufacturing: Physics of complex melt flow and formation mechanisms of pores, spatter, and denudation zones,” *Acta Materialia*, vol. 108, pp. 36–45, Apr. 2016, doi: 10.1016/j.actamat.2016.02.014.

www.manaraa.com

[20] A. Vasinonta, J. L. Beuth, and M. Griffith, "Process maps for predicting residual stress and melt pool size in the laser-based fabrication of thin-walled structures," *Journal of Manufacturing Science and Engineering, Transactions of the ASME*, vol. 129, no. 1, pp. 101–109, 2007, doi: 10.1115/1.2335852.

[21] J. Gockel, J. Beuth, and K. Taminger, "Integrated control of solidification microstructure and melt pool dimensions in electron beam wire feed additive manufacturing of ti-6al-4v," *Additive Manufacturing*, vol. 1, pp. 119–126, 2014, doi: 10.1016/j.addma.2014.09.004.

[22] D. Hu and R. Kovacevic, "Modelling and measuring the thermal behaviour of the molten pool in closed-loop controlled laser-based additive manufacturing," *Proceedings of the Institution of Mechanical Engineers, Part B: Journal of Engineering Manufacture*, vol. 217, no. 4, pp. 441–452, 2003, doi: 10.1243/095440503321628125.

[23] A. Heralić, A. K. Christiansson, M. Ottosson, and B. Lennartson, "Increased stability in laser metal wire deposition through feedback from optical measurements," *Optics and Lasers in Engineering*, vol. 48, no. 4, pp. 478–485, Apr. 2010, doi: 10.1016/j.optlaseng.2009.08.012.

[24] D. Hu and R. Kovacevic, "Sensing, modeling and control for laser-based additive manufacturing," *International Journal of Machine Tools and Manufacture*, vol. 43, no. 1, pp. 51–60, Jan. 2003, doi: 10.1016/S0890-6955(02)00163-3.

[25] M. Khanzadeh, S. Chowdhury, M. Marufuzzaman, M. A. Tschopp, and L. Bian, "Porosity prediction: Supervised-learning of thermal history for direct laser deposition," *Journal of Manufacturing Systems*, vol. 47, no. April, pp. 69–82, 2018, doi: 10.1016/j.jmsy.2018.04.001.

[26] S. H. Seifi, W. Tian, H. Doude, M. A. Tschopp, and L. Bian, "Layer-Wise Modeling and Anomaly Detection for Laser-Based Additive Manufacturing," *Journal of Manufacturing Science and Engineering, Transactions of the ASME*, vol. 141, no. 8, pp. 1–12, 2019, doi: 10.1115/1.4043898.

[27] M. Khanzadeh, S. Chowdhury, L. Bian, and M. A. Tschopp, "A methodology for predicting porosity from thermal imaging of melt pools in additive manufacturing thin wall sections," *ASME 2017 12th International Manufacturing Science and Engineering Conference, MSEC 2017 collocated with the JSME/ASME 2017 6th International Conference on Materials and Processing*, vol. 2, no. June, 2017, doi: 10.1115/MSEC2017-2909.

[28] B. M. Colosimo and M. Grasso, "Spatially weighted PCA for monitoring video image data with application to additive manufacturing," *Journal of Quality Technology*, vol. 50, no. 4, pp. 391–417, 2018, doi: 10.1080/00224065.2018.1507563.

www.manaraa.com

[29] H. Yan, M. Grasso, K. Paynabar, and B. M. Colosimo, “Real-time Detection of Clustered Events in Video-imaging data with Applications to Additive Manufacturing,” Apr. 2020, Accessed: May 13, 2020. [Online]. Available: http://arxiv.org/abs/2004.10977.

[30] S. Damas, O. Cordón, and J. Santamara, “Medical image registration using evolutionary computation: An experimental survey,” *IEEE Computational Intelligence Magazine*, vol. 6, no. 4. pp. 26–42, Nov. 2011, doi: 10.1109/MCI.2011.942582.

[31] C. J. Paciorek and M. J. Schervish, “Nonstationary Covariance Functions for Gaussian Process Regression.” Accessed: May 13, 2020. [Online].

[32] M. Seeger, “Gaussian processes for machine learning.,” *International journal of neural systems*, vol. 14, no. 2. World Scientific Publishing Company , pp. 69–106, Nov. 21, 2004, doi: 10.1142/S0129065704001899.

[33] “An Introduction to Support Vector Machines and Other Kernel-based Learning ... - Nello Cristianini, John Shawe-Taylor, Department of Computer Science Royal Holloway John Shawe-Taylor - Google Books.” (accessed May 13, 2020).

[34] M. Khanzadeh, S. Chowdhury, M. A. Tschopp, H. R. Doude, M. Marufuzzaman, and L. Bian, “In-situ monitoring of melt pool images for porosity prediction in directed energy deposition processes,” *IISE Transactions*, vol. 51, no. 5, pp. 437–455, May 2019, doi: 10.1080/24725854.2017.1417656.

www.manaraa.com